

Diffusion-induced bias in near-wall velocimetry

REZA SADR¹, CHRISTEL HOHENEGGER²,
HAIFENG LI³, PETER J. MUCHA^{2,4} AND MINAMI YODA³

¹G. W. Woodruff School of Mechanical Engineering,
Georgia Institute of Technology Savannah, Savannah, GA 31407, USA

²Department of Mathematics, University of North Carolina, Chapel Hill, NC 27599-3250, USA

³G. W. Woodruff School of Mechanical Engineering,
Georgia Institute of Technology, Atlanta, GA 30332-0405, USA

⁴Institute for Advanced Materials, University of North Carolina, Chapel Hill, NC 27599-3290, USA

(Received 7 July 2006 and in revised form 9 January 2007)

The Brownian fluctuations of the colloidal tracers often used in microscale velocimetry are typically isotropic in the bulk. In the near-wall region, however, these fluctuations are strongly affected by the hydrodynamic interaction with the wall and by the no-flux condition imposed by the wall. These wall effects can, under appropriate conditions, bias measurements based on colloidal tracers, potentially leading to significant overestimation of near-wall velocities. We use a Fokker–Planck description to generate probability density functions of the distances from a single wall sampled by the matched particles that are present in the same window at both the start and end of a time interval. The importance of the resulting bias for experimental parameters is then quantified in terms of the size of the imaged region and measurement interval. We conclude with a brief discussion of the implications for near-wall velocimetry measurements.

1. Introduction

The no-slip boundary condition at the interface between a flowing fluid and a solid wall has been a fundamental assumption of fluid dynamics since the boundary-layer theory of Prandtl. Although molecular dynamics simulations have demonstrated the validity of this condition (Koplik, Banavar & Willemsen 1989), it is nevertheless an empirical boundary condition based upon the assumption that the fluid and solid molecules behave in a similar fashion. Recently, several experimental and numerical studies have reported evidence that the no-slip condition does not hold for flow of Newtonian liquids over non-wetting and, in some cases, wetting surfaces. For one-dimensional flow past a solid stationary surface, the Navier boundary condition on the velocity u at the wall ($z=0$) with slip length b can be expressed in terms of the velocity derivative normal to the wall as $u(0) = b(\partial u / \partial z)|_{z=0}$. Non-zero b have been reported for molecular dynamics simulations of Lennard–Jones fluids (Thompson & Troian 1997; Barrat & Bocquet 1999; Galea & Attard 2004) and various experimental studies where b is inferred indirectly from viscous force or pressure drop measurements for a known (or assumed) velocity profile (Churaev, Sobolev & Somov 1984; Craig, Neto & Williams 2001; Zhu & Granick 2001, 2002; Choi, Westin & Breuer 2003). Non-zero slip lengths have also been found by linearly extrapolating measured velocities to zero. These velocities have been measured, mainly for Poiseuille flow,

using techniques including hot-film anemometry (Watanabe, Udagawa & Udagawa 1999), total-internal-reflection fluorescence recovery after photo-bleaching (Pit, Hervet & Léger 2000), microscale particle-image velocimetry (μ PIV) (Tretheway & Meinhardt 2002; Joseph & Tabeling 2005) and fluorescence cross-correlation spectroscopy (FCS) (Lumma *et al.* 2003). In all of these studies, the reported slip lengths have been less than $1\ \mu\text{m}$, suggesting that any breakdown of the no-slip condition will be significant only for micro-(and nano-)scale flows.

Most, if not all, velocimetry techniques with the spatial resolution required to obtain velocity profiles within microflows (e.g. μ PIV and FCS) measure the displacements of colloidal particles or molecular tracers over a known time interval. These techniques obtain fluid velocities by assuming that tracers follow the fluid with good fidelity. Yet several of the experimental measurements of velocity profiles using particle tracers have had difficulties with near-wall data. Because of such issues, the recent μ PIV studies of Joseph & Tabeling (2005) ignored all data within $0.5\ \mu\text{m}$ (or more) of the wall, reporting slip lengths of less than $100\ \text{nm}$ ($\pm 100\ \text{nm}$) for water flowing over hydrophilic and hydrophobic surfaces using $0.1\text{--}0.2\ \mu\text{m}$ diameter fluorescent particles. Lumma *et al.* (2003) reported that their values for b obtained from $40\ \text{nm}$ tracer particles of $\sim 1\ \mu\text{m}$ were significantly greater than those from molecular tracers under otherwise identical conditions. They attributed most of this discrepancy to particle-wall electrostatic repulsion since the discrepancy increased when NaCl was added to the molecular tracer solution. Lauga (2004) derived a model demonstrating that particle electrophoresis could also lead to larger b , but the model gave unrealistically large ζ -potential magnitudes of $300\ \text{mV}$ for $b \approx 1\ \mu\text{m}$, implying that only part of the discrepancy was due to electrophoresis.

This work considers instead the effect of Brownian fluctuations as influenced by a single wall on near-wall velocimetry using colloidal tracers. The particle distribution due to diffusion, hindered or not, made spatially asymmetric by the no-flux wall condition, must be considered for all colloidal tracers, including particles without surface charge and molecular tracers. Such effects become particularly significant when following a tracer of (effective hydrodynamic) radius a in a region of interest with wall-normal dimension $Z = O(a)$ over intervals comparable with the time to diffuse over a . We expect that spatially asymmetric sampling due to diffusion will become a major issue for micro- and nano-fluidic diagnostics in view of the increasing use of tracers such as quantum dots (QDs) (Pouya *et al.* 2005) and phosphorescent supramolecules (Maynes & Webb 2002; Lum 2005) with $a \leq O(10\ \text{nm})$ and the correspondingly long exposure times required to obtain detectable signals from such small tracers. Detailed quantification of this effect is thus potentially valuable in interpreting such experimental measurements. Lumma *et al.* (2003), for example, estimated the Brownian effects using the results of Saffman (1962) on dispersion of ground-released particles. In contrast, we include effects due to the out-of-plane spatial extent of the imaged region and near-wall hindered diffusion to provide a more accurate analysis specific to near-wall velocimetry.

Section 2 gives the Fokker–Planck description and the resulting probability density functions (PDFs) of the positions sampled by ‘matched’ tracers subject to Brownian diffusion. Sections 3 and 4 present the PDFs in terms of dimensionless variables, the large-window limiting behaviour of the PDFs, and an empirical approximation for the average sampled distance from the wall based on these PDFs. Section 5 illustrates the role of diffusion-induced bias in evanescent wave-based PIV (Sadr *et al.* 2004), while § 6 concludes with a brief consideration of the implications of this work.

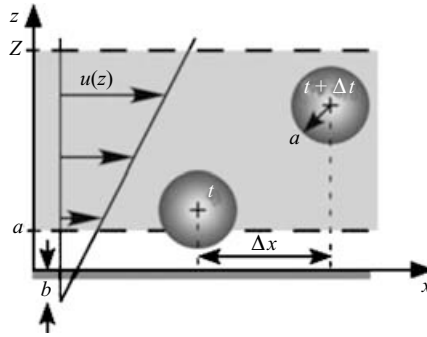


FIGURE 1. Two exposures of a particle in the near-wall region subject to the velocity $u(z)$.

2. Distribution of matched Brownian particles near the wall

Particle-based velocimetry techniques determine fluid flow velocities from an estimate of the displacement of tracer particles of radius a imaged in some region ('window'), here $a \leq z \leq Z$, between two instants in time (exposures) t and $t + \Delta t$ (figure 1). Consider particles following a one-dimensional shear flow $u(z) = G(z + b)$ with strain rate G . We assume here that the particles are uniformly distributed, the exposure time is much less than Δt , and particles are 'imaged' only if the z -location of their centres satisfies $a \leq z \leq Z$. If the measured velocity U_M is dominated by the dynamics of 'matched' particles, i.e. particles that are imaged in both exposures, U_M is a good approximation (within experimental error) of the velocity $\langle u(z) \rangle$ sampled by these particles averaged over the time interval Δt . For the shear flow

$$U_M \equiv \frac{\Delta x}{\Delta t} = \langle u(z) \rangle = G(\langle z \rangle + b) \quad (2.1)$$

the velocity sampled by these tracers can be described in terms of $\langle z \rangle$, the average z -position of matched particles over the time interval Δt .

If the matched particles remain uniformly distributed within $a \leq z \leq Z$ over Δt , $\langle z \rangle$ is then at the centre of the region, $z_c = (Z + a)/2$, and $\langle z \rangle / z_c = 1$. However, a particle in $a \leq z \leq Z$ at times t and $t + \Delta t$ can sample positions $z > Z$ during the intervening period. Hence $\langle z \rangle$ does not necessarily coincide with z_c .

The average $\langle z \rangle$ fully quantifies this effect for linearly varying near-wall velocity profiles, while higher moments of z are required for more complicated profiles $u(z)$. We note, however, that many near-wall velocity profiles can be approximated as linear; the parabolic profile across a $10 \mu\text{m}$ channel is essentially linear over the first $O(0.1 \mu\text{m})$ next to the wall, for example. It is well-known that the hydrodynamic interaction of a particle with the wall causes the particle to 'lag' behind the fluid (as described by Goldman, Cox & Brenner 1967, among others). For our analysis, however, we need only assume that there is a known particle velocity $u(z)$ in addition to Brownian motion, and that there is a well-characterized relationship between this $u(z)$ and the actual fluid velocity. The average $\langle z \rangle$ sampled by matched particles then describes the lowest-order correction due to this diffusive effect. More detailed averages of a specific $u(z)$ form can then be obtained from the probability density function described in detail below.

We model the particle behaviour as a one-dimensional diffusion process normal to the wall, i.e. along z , of non-interacting spheres, which is sufficient to correctly characterize the average particle displacements in x for $u(z)$ unidirectional flows. In contrast, full analysis of higher moments in x would require considering the

full multidimensional problem (e.g. Saffman 1962). The Stokes–Einstein diffusion coefficient in an unbounded flow $D_\infty = kT/(6\pi\mu a)$ accurately describes motion far from the walls, where k is the Boltzmann constant, T the absolute temperature and μ the fluid viscosity (Einstein 1905). The presence of the wall hinders the diffusion normal and parallel to the wall at different rates, described by correction factors β_\perp and β_\parallel , respectively (Clark, Lal & Watson 1987; Brenner 1961). Bevan & Prieve (2000) used a regression of the series expansion in z/a of Brenner (1961) to approximate the hindered diffusion coefficient along z as

$$D_\perp(z) = D_\infty \beta_\perp(z) = D_\infty \frac{6z^2 - 10az + 4a^2}{6z^2 - 3az - a^2}. \quad (2.2)$$

There are two approaches for numerically determining the z -positions sampled by matched particles: Langevin and Fokker–Planck. The Langevin approach describes the trajectory of each particle over the time interval using stochastic differential equations (for example, as in Sadr, Li & Yoda 2005*b*), while the Fokker–Planck description captures the evolution of the probability distribution of the z -positions.

The Langevin approach requires some care near the wall because numerical errors can push particles through the wall even though $D_\perp = 0$ at $z = a$, (2.2), and there should therefore automatically be zero flux across this boundary. Because the usual lowest-order Euler–Maruyama scheme occasionally pushes particles through the wall, it becomes tempting to worry about the impact of different particle–wall interaction models. However, a Milstein scheme of strong order one is equally easy to implement in one dimension (e.g. Higham 2001) and is observed to virtually eliminate this flux for reasonably small time steps (Hohenegger 2006). Hence, direct contact between particle and wall is only a numerical artifact, and the idealized model considering only hydrodynamic interaction with a smooth wall should have no particle–wall collisions.

Given that our focus here is on averaged quantities such as $\langle z \rangle$, it is more efficient to work in the Fokker–Planck framework. Assuming all particles are identical, consider a single colloidal particle subject to position-dependent non-inertial hydrodynamic interactions with the wall, in the absence of all other interacting or external forces. Assuming that time scales of interest are much longer than the momentum relaxation time (e.g. Ermak & McCammon 1978), the evolution of the average density $f(z, t)$ of particles with centres at distance z normal to the wall at time t reduces to a configuration-space Fokker–Planck (or Smoluchowski) description equivalent to a heat equation with non-uniform conductivity in a semi-infinite rod:

$$\frac{\partial f(z, t)}{\partial t} = \frac{\partial}{\partial z} \left(D_\perp(z) \frac{\partial f(z, t)}{\partial z} \right), \quad (2.3)$$

subject to the condition that such particles are initially uniformly distributed in the imaged region at $t = 0$ (in the absence of other interactions which might skew this distribution) and the Neumann boundary condition of zero flux at the wall ($z = a$):

$$f(z, 0) = \frac{\chi(z)}{Z - a} \quad \text{where} \quad \chi(z) = \begin{cases} 1 & \text{if } a \leq z \leq Z \\ 0 & \text{otherwise,} \end{cases} \quad D_\perp(z) \frac{\partial f}{\partial z} \Big|_{z=a} = 0. \quad (2.4)$$

Since $\beta_\perp \rightarrow 0$ at the wall, the Neumann boundary condition is automatically satisfied for all well-behaved $f(z, t)$. We note that inclusion of other forces on the particles changes (2.3) and both the boundary condition and presumed steady-state particle distribution from which particles are initially drawn in (2.4); such influences change the details of our results below, proper calculation of the probability density function

(PDF) then requiring solutions of the appropriate adjoint equations (see, e.g., the classic reprinted text by Lanczos 1997).

The particle density $f(z, t)$ defined above includes all the particles originally in the imaged region ($a \leq z \leq Z$). The measured velocities of these particles, however, depend on the PDF $P(z)$ of distances from the wall z that are sampled by *matched* particles during the interval Δt , the matched particles being those that are physically present in the imaged region at both the beginning and end of the interval, i.e. times 0 and Δt . This PDF is constructed from the product of the probabilities of Brownian paths that: (i) begin uniformly in the imaged region at time 0 and end at intermediate space–time point (z, t) ; and (ii) begin at (z, t) and end in the imaged region at time Δt (note $0 \leq t \leq \Delta t$). The first of these probabilities is $f(z, t)$, by definition. The second is, by a standard calculation reproduced in the Appendix, proportional to $f(z, \Delta t - t)$. The density of matched particles at any space–time point (z, t) , $0 \leq t \leq \Delta t$, is hence equal to $kf(z, t)f(z, \Delta t - t)$, where k is a constant determined by the fraction of particles in the imaged region at time 0 that are also in the imaged region at time Δt . The PDF of z -positions sampled by matched particles during the time interval is then this density averaged over Δt :

$$P(z) = K \int_0^{\Delta t} f(z, t) f(z, \Delta t - t) dt, \quad (2.5)$$

with the normalization constant K defined so that $\int_a^\infty P(z) dz = 1$. We have confirmed that (2.5) gives PDFs of matched particles identical (within statistical noise) to those obtained directly from Langevin simulations (Sadr *et al.* 2005*b*) across a wide range of parameters. Finally, the average z -position of the matched particles is

$$\langle z \rangle = \int_a^\infty z P(z) dz. \quad (2.6)$$

Equation (2.3) subject to (2.4) was solved numerically on domains $a \leq z \leq L$ (L large) using adaptively selected time steps, and selected fine spatial discretizations so that the numerical parameters had little effect on the solutions. The integrations in (2.5) and (2.6) were performed using finely discretized trapezoidal rules for simplicity, also tested for numerical convergence.

3. Dimensional analysis and results

The PDF $P(z)$ depends on the physical parameters ($a, Z, D_\infty, \Delta t$) as well as the particle-centre–wall distance z . These quantities in basic dimensions of length and time can be reduced to three dimensionless variables:

$$\zeta = \frac{z - a}{Z - a}, \quad W = \frac{Z - a}{a}, \quad \Omega = \frac{D_\infty \Delta t}{Z^2}, \quad (3.1)$$

the dimensionless window-edge–wall distance, window width, and time interval, respectively. Note that time is normalized here by the characteristic time taken to diffuse across a region of thickness Z . While the time taken to diffuse across the particle radius a may seem a more natural choice of time scale (e.g. Sadr, Li & Yoda 2005*a*), the choice in (3.1) is better-suited to the calculation here where we are mainly interested in tracer motion across $O(Z)$ distances. As shown subsequently, this choice describes well the diffusion bias behaviour over a wide range of parameters.

$\mathcal{P}(\zeta, \Omega, W)$ represents the PDF of dimensionless edge–wall distances sampled by matched particles imaged in the region $0 \leq \zeta \leq 1$. That is, a particle is matched if

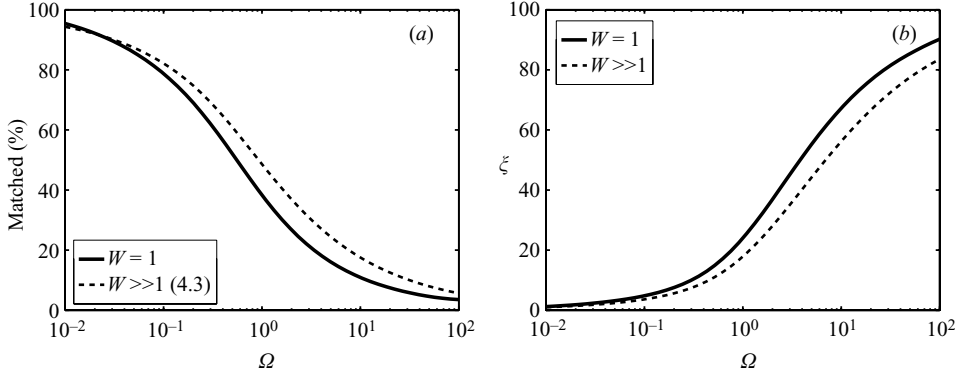


FIGURE 2. (a) Percentage of particles that are matched as a function of Ω for $W=1$ or $a \leq z \leq 2a$ (solid curve), and by (4.3) for the $W \gg 1$ limit (dashed line). (b) Average percentage of time-matched particles spend sampling at distances $\zeta > 1$, as a function of Ω , for $W=1$ (solid line) and for the $W \gg 1$ limit (dashed line) computed using (4.2).

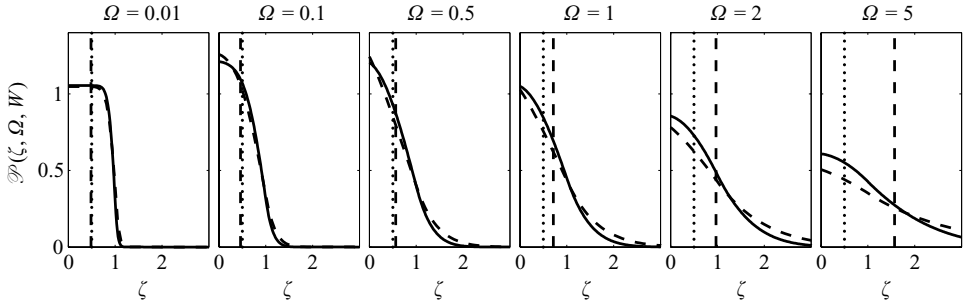


FIGURE 3. PDFs of the positions sampled by matched particles at different values of Ω for $W=1$ (dashed curves) and $W=8$ (solid curves), with mean sampled positions $\langle \zeta \rangle$ for $W=1$ at each time given by a vertical dashed line. The geometric centre of the imaged region, $\zeta=0.5$, is indicated by a vertical dotted line.

$0 \leq \zeta \leq 1$ at non-dimensional times 0 and Ω . Given the small extent of the window, many particles present in the window in the first exposure (initial time 0) ‘drop out’, i.e. have diffused out of the window by the second exposure (dimensionless time Ω), leading to significant particle mismatch. Figure 2(a) shows the number of matched particles, as a fraction of the tracers present in the first exposure, as a function of the dimensionless time interval Ω for a window of width $W=1$ and the $W \gg 1$ limit (cf. section 4); less than 50% and 20% of the particles are matched for time intervals $\Omega=1$ and 10, respectively.

Figure 2(a) shows that the majority of particles drop out for intervals $\Omega > 1$. Particles can also, however, leave the window at intermediate times and still be matched if they return to the window by time Ω . Figure 2(b) shows ξ , the average fraction of the time interval that *matched* particles are outside the window (i.e. $\zeta > 1$) as a function of Ω . As Ω increases, matched particles spend more time at $\zeta > 1$, with $\xi \approx 20\%$ and $\xi > 60\%$ for $\Omega=1$ and 10, respectively.

Figure 3 shows PDFs of the positions sampled by matched particles at several Ω for windows of width $W=1$ (dashed lines) and 8 (solid lines); $\langle \zeta \rangle$ for each $W=1$ case is denoted by a vertical dashed line. Note that $W=1$ corresponds to a window $a \leq z \leq 2a$, and illustrates typical behaviour for small windows, while the $W=8$ case

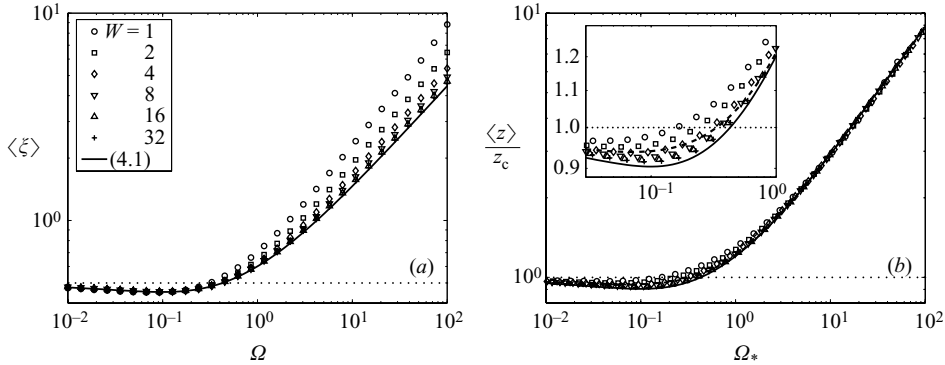


FIGURE 4. (a) $\langle \zeta \rangle$ vs. Ω . (b) $\langle z \rangle / z_c$ vs. Ω_* . The dashed line denotes the fit (4.6).

exemplifies behaviour for large windows, as further discussed below. Most tracer-based velocimetry techniques assume $\langle \zeta \rangle = 0.5$, corresponding to the centre of the window. But as Ω increases, $\langle \zeta \rangle$ shifts first to the left, becoming slightly less than 0.5, before shifting to the right, increasing indefinitely with increasing Ω .

At small Ω , particles near the $\zeta = 1$ edge of the window can become mismatched by diffusing out of the window. However, the particles cannot leave the window through the ‘touching-the-wall’ edge at $\zeta = 0$, due to the no-flux condition. The resultant reduction in the number of matched particles near $\zeta \approx 1$ shifts the matched particle distribution to the left (i.e. reduces $\langle \zeta \rangle$) because a PDF is, by definition, normalized to have an area of 1. As Ω increases, more matched particles will sample distances outside the window, shifting the mean to higher values until $\langle \zeta \rangle > 0.5$, as observed for $\Omega \geq 0.5$ in figure 3.

The figure also demonstrates that the main trends in the PDFs are only weakly dependent on W , since most of the window-size diffusive effects are already accounted for in the selected definition of Ω . The discrepancies in the PDFs at different W are mainly due to near-wall differences in the relative effect of hindered diffusion, which is more significant for small W .

4. Modelling

Figure 3 shows that $\langle \zeta \rangle$ can exceed 0.5 for $\Omega \geq 0.5$, that is, Brownian diffusion can lead to overestimation of near-wall velocities for intervals $\Delta t \sim Z^2/D_\infty$, the tracer diffusion time. Figure 4(a) plots $\langle \zeta \rangle$ vs. Ω for various values of W . The results for $W \geq 8$ tend to the solid curve, which is an independent calculation for $\langle \zeta \rangle$ in the $W \gg 1$ limit. In this limit, the window is so large that the effects of hindered diffusion are negligible, and the diffusion coefficient limits to D_∞ everywhere. The average position of the particles for $W \gg 1$ is then

$$\langle \zeta \rangle_\infty = \frac{1}{\Omega} \int_0^\Omega d\Omega' \int_0^\infty d\zeta \zeta f_\infty(\zeta, \Omega') f_\infty(\zeta, \Omega - \Omega'), \quad (4.1)$$

with

$$f_\infty(\zeta, \Omega) = \frac{1}{2F_\infty} \left(\operatorname{erf} \left[\frac{\zeta + 1}{2\sqrt{\Omega}} \right] - \operatorname{erf} \left[\frac{\zeta - 1}{2\sqrt{\Omega}} \right] \right) \quad (4.2)$$

and

$$F_\infty = \frac{1}{2} \int_0^1 d\zeta \left(\operatorname{erf} \left[\frac{\zeta + 1}{2\sqrt{\Omega}} \right] - \operatorname{erf} \left[\frac{\zeta - 1}{2\sqrt{\Omega}} \right] \right) = \operatorname{erf} \left[\frac{1}{\sqrt{\Omega}} \right] + (e^{-1/\Omega} - 1) \sqrt{\frac{\Omega}{\pi}}. \quad (4.3)$$

The integrals in (4.1) can be evaluated numerically. The fraction of matched particles for $W \gg 1$, $F_\infty(\Omega)$, is shown in figure 2(a); the average time that matched particles spend outside the window for $W \gg 1$,

$$\xi_\infty = \frac{1}{\Omega} \int_0^\Omega d\Omega' \int_1^\infty d\zeta f_\infty(\zeta, \Omega') f_\infty(\zeta, \Omega - \Omega') \quad (4.4)$$

is given in figure 2(b).

Figure 4(a) shows that $\langle \zeta \rangle$ is effectively independent of W for short intervals, e.g. $\Omega < 0.2$. While $\langle \zeta \rangle \rightarrow 0.5$ as $\Omega \rightarrow 0$ (as expected, since the geometric centre of the imaged region is at $\zeta = 0.5$), $\langle \zeta \rangle$ becomes less than 0.5 as Ω increases, corresponding to the shift to the left observed in figure 3, reaching a minimum value of about 0.46. Finally, $\langle \zeta \rangle$ becomes greater than 0.5 for $\Omega \geq 0.5$, increasing monotonically with Ω . At a given Ω , $\langle \zeta \rangle$ increases as W decreases because of the precise non-dimensionalization choice (3.1) used here. We caution, however, that for the applications in microchannels the $W \gg 1$ ‘limit’ must be interpreted with some care, since the single-wall analysis is only valid when both Z and $\langle z \rangle$ are both much smaller than the channel dimensions.

Next, consider the normalized average centre position of the matched particles, $\langle z \rangle / z_c$, where the average centre position

$$\langle z \rangle = a (W \langle \zeta \rangle + 1) \quad (4.5)$$

determines the measured velocity in a given shear flow (2.1). Recognizing that the $W \gg 1$ limiting curve is insensitive to details in defining lengths of $O(a)$, we consider whether an alternative time scale choice further collapses the long-time behaviours. While $Z - a$ is the true extent of the z -positions that can be sampled by the tracers in the window, the near-wall hindered diffusion more strongly influences results for small windows. One could then choose to rescale time as if regions of depth Z had an approximate effective diffusive length $Z + Ka$ for some constant K , giving non-dimensional time intervals $\Omega_* = D_\infty \Delta t / (Z + Ka)^2$. A choice of constant $K = 0.8$ (to one significant digit) minimizes the $\langle z \rangle / z_c$ variation at a given Ω_* over the range of W considered here for $\Omega_* > 1$, as shown in figure 4(b). The greatest variation in the data at a given Ω_* of $\sim 7\%$ occurs for $\langle z \rangle < z_c$ or $\Omega_* < 1$. This ‘error’ can be further reduced by noting (figure 4a) that $\langle \zeta \rangle$ is well-approximated in this range in terms of Ω by the $W \gg 1$ limiting curve (4.1), and using (4.5) to then estimate $\langle z \rangle$.

Finally, we empirically approximate the $W \gg 1$ limiting curve (4.1) (vs. an exact calculation using numerical integration) based on two observations. First, as already remarked, the dominant process at short times is that unmatched particles originate almost exclusively well away from the wall. As a diffusive process, the short-time deficit in $\langle z \rangle$ compared with z_c then scales as the square-root of time. The long-time behaviour of $\langle z \rangle$ is dictated by the diffusion of matched particles into and out of the imaged region within Δt , and hence also scales as square-root of time. We therefore propose the simple empirical approximation

$$\frac{\langle z \rangle}{z_c} \approx F(\Omega_*) = A + (1 - A) \exp \{-B \sqrt{\Omega_*}\} + C \sqrt{\Omega_*}. \quad (4.6)$$

To maximize the utility of this approximation at small W , a nonlinear least-squares curve was fitted to the data in figure 4(b) (instead of fitting to the limiting curve itself), giving $A = 0.21$, $B = 1.72$, $C = 0.86$ (dashed curve). This fit (4.6) is everywhere within about 7% and 5% of the actual values of $\langle z \rangle / z_c$ for $W = 1$ and $W \geq 2$, respectively, with the largest relative errors occurring at $\Omega_* \sim 0.2$ (figure 4b, inset).

We note that the large-time limit of this analysis is verified by the analysis of Saffman (1962), as used by Lumma *et al.* (2003) to estimate the bias effect of Brownian diffusion. Saffman described the Taylor dispersion of tracers released at a single point at the ground ($z=0$) and blown by the wind, modelled as a shear flow of semi-infinite extent. The constant-diffusion part of his analysis included the calculation of the average displacement of particles near the ground, indicating an additional downwind displacement with effective velocity that scaled as \sqrt{t} . As proposed by Lumma *et al.*, this analysis can be used to estimate the effect of interest here, but this point-source estimate ignores both hindered diffusion and the non-zero spatial extent of the imaged region (Z) and is hence only accurate at large times, when the diffusion distances are much greater than Z , i.e. $\Omega \gg 1$. The use of the Saffman result in the present context is equivalent to $\langle z \rangle / z_c = 1 + \frac{1}{2} \sqrt{\pi \Omega}$. Although this result agrees with (4.6) in the $\Omega_* \gg 1$ limit (for $C = \sqrt{\pi}/2 \doteq 0.886$), using the Saffman result significantly overestimates the bias due to Brownian diffusion for $\Omega \lesssim O(1)$ intervals comparable to the time to diffuse over $O(Z)$ distances.

5. Application to multilayer nPIV

We first observed Brownian diffusion-induced bias while developing ‘multilayer nano-PIV’ (mnPIV) (Li, Sadr & Yoda 2006). ‘Standard’ nano-PIV (nPIV) uses evanescent-wave illumination of colloidal particles to measure the velocity components tangential to and within ~ 250 nm of the wall (Sadr *et al.* 2004). The brightness of the particle image should be a function of its distance z normal to the wall for monodisperse particles because the intensity of this illumination decays exponentially with z . Since commercially available colloidal tracers have up to 10% polydispersity and hence significant variation in image intensity even at the same z , mnPIV ‘bins’ particle images into only a few layers based upon their brightness.

In their initial studies, Li *et al.* (2006) analysed noisy artificial images of $a = 50$ nm spheres illuminated by evanescent waves subject to hindered Brownian diffusion and shear flow with $G = 3000 \text{ s}^{-1}$ and $b = 0$. Multilayer nPIV was used to divide particle images within ~ 350 nm of the wall into three adjacent layers. While studying the effect of the time interval Δt between images within each image pair, they observed in the first layer (I) next to the wall with $Z = 80$ nm (corresponding to $W = 0.6$) that $\langle z \rangle / z_c$ increased monotonically from 1.1 at $\Omega = 0.8$ to 1.4 at $\Omega = 3.2$.

Figure 5(a) shows $\langle z \rangle / z_c$ calculated using the Fokker–Planck approach described in §2 as a function of $D_\infty \Delta t / a^2$ for each of the three layers considered by Li *et al.*: (I) $1 \leq z/a \leq 1.6$, (II) $1.6 \leq z/a \leq 2.7$, (III) $2.7 \leq z/a \leq 7$. Note that we use a instead of Z as the length scale here because layers II and III do not ‘start’ at the wall, and Z is hence undefined for these cases. Furthermore, the Fokker–Planck results for layers II and III were obtained using initial conditions appropriate for these layers, not (2.4). We only consider the effect of near-wall Brownian diffusion on mnPIV here, ignoring the effects of the non-uniform illumination.

The agreement between the two sets of results for layers I and II suggests that the increase in $\langle z \rangle / z_c$ with Δt for these two layers, especially for layer I, is primarily due to diffusion-induced bias, and, as discussed previously, that this bias is most significant in the layer immediately next to the wall. Figure 5(b) shows the layer I results normalized by $F(\Omega_*)$, the empirical approximation (4.6), as a function of Ω_* (the empirical approximation is valid only for imaged regions immediately adjacent to the wall, i.e. layer I here). The approximation does surprisingly well, estimating $\langle z \rangle / z_c$ within 10% over the entire range of Ω_* , even for this small window ($W = 0.6$) where (4.6) is expected to be relatively inaccurate (cf. $W = 1$ results in figure 4b).

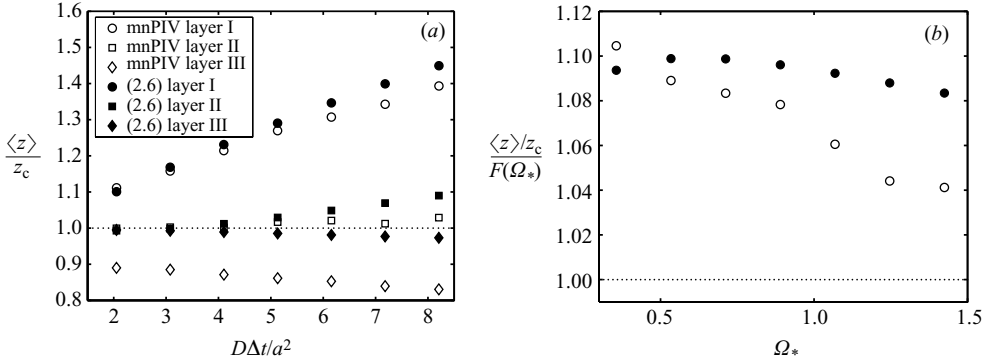


FIGURE 5. (a) $\langle z \rangle / z_c$ vs. $D\infty\Delta t/a^2$ for the mnPIV parameters of Li *et al.* (2006) calculated from the PDFs (closed symbols) and artificial images (open symbols, Li *et al.* 2006) for layers I (\circ), II (\square) and III (\diamond). (b) $\langle z \rangle / z_c$ normalized by $F(\Omega_*)$ vs. Ω_* for layer I (PDFs, closed; artificial images, open), with $F(\Omega_*)$ given by (4.6).

Figure 5(b) demonstrates the value of the empirical approximation (4.6) in estimating the significance of Brownian diffusion-induced bias over a wide range of parameters for the region where this bias is greatest, i.e. immediately adjacent to the wall. Furthermore, the differences between our results and those of Li *et al.* for layer III suggest that most of the decrease in $\langle z \rangle / z_c$ observed by Li *et al.* is due to the non-uniform illumination.

6. Implications

We conclude with some implications of this work for other near-wall velocimetry studies. This single-wall analysis is valid only when other geometric effects are relatively unimportant, for instance when the window size $Z \ll h$, the microchannel half-height, and the interval between exposures $\Delta t \ll T_{cr}$, the time required for a tracer to diffuse across distance z of, say, $0.1h$, or $T_{cr} \equiv 0.01h^2/D_\infty$ (in dimensionless variables, $\Omega \ll 0.01h^2/Z^2$).

Lumma *et al.* (2003), who used FCS to study Poiseuille flow through $h = 55 \mu\text{m}$ microchannels, reported differences of $O(100 \text{ nm})$ in slip length b when using particle rather than molecular, tracers. FCS differs from PIV in that it correlates spatially averaged signals from several tracers passing through two distinct roughly cylindrical regions separated by a known distance. The present PIV-based analysis of matched particles across a specified time interval is therefore not directly applicable to FCS. Nevertheless, a rough estimate of the effect of sampling different z distances can be obtained for their experimental parameters of $a = 20 \text{ nm}$, $Z = 800 \text{ nm}$ (i.e. half their reported depth of focus) and using $\Delta t \approx 50 \text{ ms}$ (vs. $T_{cr} \approx 2.5 \text{ s}$), giving $\Omega \approx 0.9$. This assumed Δt is, however, much greater than the estimated transit time for a single particle near the wall of $\sim 2 \text{ ms}$, but much less than the total data acquisition times reported. While not a precise analysis, this estimate thus suggests that their results are no more than weakly affected by Brownian diffusion-induced bias. Although Lumma *et al.* concluded that such effects (‘Taylor slip’) could account for nearly all of the slip lengths that they measured using particle tracers, the analysis developed here indicates that the Brownian diffusion effects on a spatially distributed ‘source’ of particles, although potentially significant, may not be as great as those estimated by Lumma *et al.*, and so electrophoretic effects (Lauga 2004) could indeed account for

at least part of the differences in b . Finally, we note that our single-wall analysis is less applicable to the molecular tracer data, since $T_{\text{cr}} \approx 80$ ms (based upon $D_{\infty} = 3.6 \times 10^{-10} \text{ m}^2 \text{ s}^{-1}$), giving $\Delta t \sim T_{\text{cr}}$.

Brownian diffusion-induced bias will be most significant for small tracers. To our knowledge, the smallest ‘particle-like’ tracers used to date are the CdSe/ZnS quantum dots (QDs) utilized by Pouya *et al.* (2005) in their evanescent-wave illumination particle tracking studies in a $h = 100 \mu\text{m}$ channel. Using their experimental parameters of $a = 5.3$ nm (based upon hydrodynamic radius), $Z = 200$ nm (twice their reported penetration depth) and $\Delta t = 71$ ms (the relatively weak emission from the QDs required exposures of at least 10 ms at a framing rate of 14 Hz), vs. $T_{\text{cr}} \approx 2.2$ s, gives $\Omega \approx 80$. The results of this work, however, are not directly applicable to those experiments, where particles were tracked over several (vs. two) exposures to ensure that they were ‘matched,’ i.e. remained in the observation region with little, if any, out-of-plane motion. The analysis developed here assumes instantaneous tracer exposures, or short exposures compared to any characteristic time of tracer motion. In Pouya *et al.*, on the other hand, the 10 ms exposures themselves correspond to $\Omega > 10$. Thus, the exposure times and time intervals indicate the possibility of large diffusive excursions; but the details of the tracking protocol used by Pouya *et al.* significantly complicate the analysis considered here. Nevertheless, this large value of Ω suggests that Brownian diffusion-induced bias should be carefully considered in future PIV measurements using QD tracers.

These results show that the asymmetric and hindered nature of Brownian trajectories near the wall introduces a bias that can lead to a significant overestimation of near-wall velocities, and hence potentially an overestimation of slip length. It is unlikely that this bias explains the wide range of slip lengths reported in recent experimental studies, with the possible exception of the particle data of Lumma *et al.* (2003).

Nevertheless, it is clear that nanoflows, or flows of overall dimension less than $O(100 \text{ nm})$, are an emerging area of fluid mechanics, with applications to *in vivo* drug delivery and single-molecule detection, for example. At such scales, the entire flow can be considered ‘near-wall’, with geometry-influenced diffusion effects across most of the channel. Moreover, improving the spatial resolution of tracer-based velocimetry techniques to obtain velocity fields in such flows will require much smaller tracers with radii of a few nanometres. Imaging such tracers will require much longer exposure times, given their reduced signal, and hence larger Δt , to obtain two independent samples of tracer position. Together, these trends suggest that extending current tracer-based velocimetry techniques to such flows will probably require careful consideration of the Brownian diffusion effects, modelled here by a simple single-wall analysis, including using empirical approximations such as (4.6).

This research was supported by the Air Force Office of Scientific Research (contract FA9550-04-C-0130) and the Department of Energy (grant DE-FG-02-03ER25567). Part of this work was presented at the 6th International Symposium on Particle Velocimetry (Pasadena, CA).

Appendix. Proof

$f(z, t)$ solutions of (2.3) and (2.4) describe the probability density of Brownian paths that begin uniformly in the imaged region $a \leq z \leq Z$ at time 0 and end at space-time

point (z, t) , $0 \leq t \leq \Delta t$. The independent probability that a particle starting at (z, t) ends in the imaged region at time Δt is then

$$\Pi = \int_a^Z g(z', \Delta t - t; z) dz' \tag{A 1}$$

where $g(z', t; z)$, like $f(z, t)$, satisfies (2.3) subject to the no-flux boundary condition of (2.4) but is subject instead to the initial condition that $g(z', 0; z) = \delta(z' - z)$, the Dirac delta function. We prove in this Appendix that the probability Π can be calculated directly from the particle distribution $f(z, t)$.

Let $u(z, t)$ and $v(z, t)$ represent two solutions of (2.3) satisfying the no-flux boundary condition in (2.4) for $a \leq z \leq \infty$ with initial conditions specified at time $t = 0$. Assume that u, v and the diffusion coefficient $D(z) = D_{\perp}(z)$ all have well-behaved derivatives. We can then, by repeated integration by parts, show that the diffusion operator in (2.3) is self-adjoint:

$$\begin{aligned} \int_a^{\infty} u(z, t') \frac{\partial v(z, t)}{\partial t} dz &= \int_a^{\infty} u(z, t') \frac{\partial}{\partial z} \left(D(z) \frac{\partial v(z, t)}{\partial z} \right) dz \\ &= u(z, t') D(z) \frac{\partial v(z, t)}{\partial z} \Big|_{z=a}^{\infty} - \int_a^{\infty} \frac{\partial u(z, t')}{\partial z} D(z) \frac{\partial v(z, t)}{\partial z} dz \\ &= -D(z) \frac{\partial u(z, t')}{\partial z} v(z, t) \Big|_{z=a}^{\infty} + \int_a^{\infty} \frac{\partial}{\partial z} \left(D(z) \frac{\partial u(z, t')}{\partial z} \right) v(z, t) dz \\ \int_a^{\infty} u(z, t') \frac{\partial v(z, t)}{\partial t} dz &= \int_a^{\infty} \frac{\partial u(z, t')}{\partial t'} v(z, t) dz \end{aligned} \tag{A 2}$$

where all the boundary terms vanish because of the no-flux boundary conditions.

Setting $t' = \tau - t$, it immediately follows that the integral $\int_a^{\infty} u(z, \tau - t) v(z, t) dz$ is independent of t , $0 \leq t \leq \tau$, since the partial derivative of this integral with respect to t is identically zero from (A 2):

$$\begin{aligned} \frac{\partial}{\partial t} \int_a^{\infty} u(z, \tau - t) v(z, t) dz \\ = - \int_a^{\infty} \frac{\partial u(z, t')}{\partial t'} \Big|_{t'=\tau-t} v(z, t) dz + \int_a^{\infty} u(z, \tau - t) \frac{\partial v(z, t)}{\partial t} dz = 0. \end{aligned} \tag{A 3}$$

That is, this integral is identical for u and v evaluated at any two ‘times’ (here, $\tau - t$ and t) whose sum is a specified constant (here, τ).

Next, impose the selected initial conditions $u(z', 0) = \chi(z')$ (cf. (2.4)) and $v(z', 0) = \delta(z' - z)$. Then the probability (A 1) of a particle at (z, t) ending in the imaged region at time Δt (that is, a time $t' = \Delta t - t$ after the space–time point of interest) becomes

$$\Pi = \int_a^Z v(z', t') dz' = \int_a^{\infty} u(z', 0) v(z', t') dz' = \int_a^{\infty} u(z', t') v(z', 0) dz' \tag{A 4}$$

by (A 3). Substituting in $t' = \Delta t - t$ and the initial condition for v :

$$\Pi = \int_a^{\infty} u(z', t') \delta(z' - z) dz' = u(z, \Delta t - t) \tag{A 5}$$

where $u(z, t) = (Z - a) f(z, t)$ by definition, and $f(z, t)$ is, again, the probability density of Brownian paths that begin uniformly in the imaged region at time 0 and end at

space–time point (z, t) . So the probability that a particle starting at (z, t) ends in the imaged region at time Δt is indeed, within a multiplicative constant, equal to $f(z, \Delta t - t)$.

REFERENCES

- BARRAT, J.-L. & BOCQUET, L. 1999 Influence of wetting properties on hydrodynamic boundary conditions at fluid/solid interface. *Faraday Disc.* **112**, 119–128.
- BEVAN, M. A. & PRIEVE, D. C. 2000 Hindered diffusion of colloidal particles very near to a wall: revisited. *J. Chem. Phys.* **113**, 1228–1236.
- BRENNER, H. 1961 The slow motion of a sphere through a viscous fluid towards a plane surface. *Chem. Engng Sci.* **16**, 242–251.
- CHOI, C.-H., WESTIN, K. J. A. & BREUER, K. S. 2003 Apparent slip flows in hydrophilic and hydrophobic microchannels. *Phys. Fluids* **15**, 2897–2902.
- CHURAEV, N. V., SOBOLEV, V. D. & SOMOV, A. N. 1984 Slippage of liquids over lyophobic solid surfaces. *J. Colloid Interface Sci.* **97**, 574–581.
- CLARK, A. T., LAL, M. & WATSON, G. M. 1987 Dynamics of colloidal particles in the vicinity of an interacting surface. *Faraday Disc.* **83**, 179–191.
- CRAIG, V. S. J., NETO, C. & WILLIAMS, D. R. M. 2001 Shear-dependent boundary slip in an aqueous Newtonian liquid. *Phys. Rev. Lett.* **87**, 054504/1–4.
- EINSTEIN, A. 1905 Über die von der molekularkinetischen Theorie der Wärme geforderte Bewegung von in ruhenden Flüssigkeiten suspendierten Teilchen. *Ann. Physik* **17**, 549–560.
- ERMAK, D. L. & MCCAMMON, J. A. 1978 Brownian dynamics with hydrodynamic interactions. *J. Chem. Phys.* **69**, 1352–1360.
- GALEA, T. M. & ATTARD, P. 2004 Molecular dynamics study of the effect of atomic roughness on the slip length at the fluid–solid boundary during shear flow. *Langmuir* **20**, 3477–3482.
- GOLDMAN, A. J., COX, R. G. & BRENNER, H. 1967 Slow viscous motion of a sphere parallel to a plane wall - II: Couette flow. *Chem. Engng Sci.* **22**, 653–660.
- HIGHAM, D. J. 2001 An algorithmic introduction to numerical simulation of stochastic differential equations. *SIAM Rev.* **43**, 525–546.
- HOHENEGGER, C. 2006 Small scale stochastic dynamics for particle image velocimetry applications. PhD thesis, Georgia Institute of Technology.
- JOSEPH, P. & TABELING, P. 2005 Direct measurement of the apparent slip length. *Phys. Rev. E* **71**, 035303.
- KOPLIK, J., BANAVAR, J. R. & WILLEMSSEN, J. F. 1989 Molecular dynamics of fluid flow at solid surfaces. *Phys. Fluids A* **1**, 781–794.
- LANCZOS, C. 1997 *Linear Differential Operators*. Dover Publications (reprint).
- LAUGA, E. 2004 Apparent slip due to the motion of suspended particles in flows of electrolyte solutions. *Langmuir* **20**, 8924–8930.
- LI, H., SADR, R. & YODA, M. 2006 Multilayer nano-particle image velocimetry. *Exps. Fluids* **41**, 185–194.
- LUM, C. 2005 An experimental study of pressure- and electroosmotically-driven flows in microchannels with surface modifications. PhD thesis, Michigan State University.
- LUMMA, D., BEST, A., GANSEN, A., FEUILLEBOIS, F., RÄDLER, J. O. & VINOGRADOVA, O. I. 2003 Flow profile near a wall measured by double-focus fluorescence cross-correlation. *Phys. Rev. E* **67**, 056313.
- MAYNES, D. & WEBB, A. R. 2002 Velocity profile characterization in sub-millimeter diameter tubes using molecular tagging velocimetry. *Exps. Fluids* **32**, 3–15.
- PIT, R., HERVET, H. & LÉGER, L. 2000 Direct experimental evidence of slip in hexadecane: solid interfaces. *Phys. Rev. Lett.* **85**, 980–983.
- POUYA, S., KOCHESFAHANI, M., SNEE, P., BAWENDI, M. & NOCERA, D. 2005 Single quantum dot (QD) imaging of fluid flow near surfaces. *Exps. Fluids* **39**, 784–786.
- SADR, R., LI, H. & YODA, M. 2005a Bias due to hindered Brownian diffusion in near-wall velocimetry. *Proc. 6th Intl Symp. on Particle Image Velocimetry, Pasadena, CA*.
- SADR, R., LI, H. & YODA, M. 2005b Impact of hindered Brownian diffusion on the accuracy of particle-image velocimetry using evanescent-wave illumination. *Exps. Fluids* **38**, 90–98.

- SADR, R., YODA, M., ZHENG, Z. & CONLISK, A. T. 2004 An experimental study of electro-osmotic flow in rectangular microchannels. *J. Fluid Mech.* **506**, 357–367.
- SAFFMAN, P. G. 1962 The effect of wind shear on horizontal spread from an instantaneous ground source. *Q. J. R. Met. Soc.* **88**, 382–393.
- THOMPSON, P. A. & TROIAN, S. M. 1997 A general boundary condition for liquid flow at solid surfaces. *Nature* **389**, 360–362.
- TRETHEWAY, D. C. & MEINHART, C. D. 2002 Apparent fluid slip at hydrophobic microchannel walls. *Phys. Fluids* **14**, L9–L12.
- WATANABE, K., UDAGAWA, Y. & UDAGAWA, H. 1999 Drag reduction of Newtonian fluid in a circular pipe with a highly water-repellent wall. *J. Fluid Mech.* **381**, 225–238.
- ZHU, Y. & GRANICK, S. 2001 Rate-dependent slip of Newtonian liquid at smooth surfaces. *Phys. Rev. Lett.* **87**, 96105.
- ZHU, Y. & GRANICK, S. 2002 No-slip boundary condition switches to partial slip when fluid contains surfactant. *Langmuir* **18**, 10058–10063.